



SCC Publishing Michelets vei 8 B 1366 Lysaker Norway

ISSN: 2703-9072

Multiscale Comparative Spectral Analysis of Satellite Total Solar Irradiance Measurements from 2003 to 2013 Reveals a Planetary Modulation of Solar Activity and its Nonlinear Dependence on the 11 yr Solar cycle¹

Correspondence:
Nicola.scaf-

etta@gmail.com and rwilslson@acrim.com

> Vol. 5.2 (2025) pp. 129–147

^{a,b}Nicola Scafetta and Richard C. Willson^a

^aActive Cavity Radiometer Irradiance Monitor (ACRIM) Lab, Coronado, CA 92118, USA ^bDuke University, Durham, NC 27708

Abstract

Herein we adopt a multiscale dynamical spectral analysis technique to compare and study the dynamical evolution of the harmonic components of the overlapping ACRIMSAT/ACRIM3 (Active Cavity Radiometer Irradiance Monitor Satellite/Active Cavity Radiometer Irradiance Monitor 3), SOHO/VIRGO (Solar and Heliopheric Observatory/Variability of solar Irradiance and Gravity Oscillations), and SORCE/TIM (Solar Radiation and Climate Experiment/Total Irradiance Monitor) total solar irradiance (TSI) records during 2003.15 to 2013.16 in solar cycles 23 and 24. The three TSI time series present highly correlated patterns. Significant power spectral peaks are common to these records and are observed at the following periods: $\sim 0.070 \text{ yr}, \sim 0.097 \text{ yr}, \sim 0.20$ yr, ~ 0.25 yr, ~ 0.30 –0.34 yr, and ~ 0.39 yr. Less certain spectral peaks occur at about 0.55 yr, 0.60-0.65 yr and 0.7-0.9 yr. Four main frequency periods at ~ 24.8 days (~ 0.068 yr), ~ 27.3 days (~ 0.075 yr), at $\sim 34-35$ days ($\sim 0.093-0.096$ yr), and $\sim 36-38$ days ($\sim 0.099-0.104$ yr) characterize the solar rotation cycle. The amplitude of these oscillations, in particular of those with periods larger than 0.5 yr, appears to be modulated by the ~ 11 yr solar cycle. Similar harmonics have been found in other solar indices. The observed periodicities are found highly coherent with the spring, orbital and synodic periods of Mercury, Venus, Earth and Jupiter. We conclude that solar activity is likely modulated by planetary gravitational and electromagnetic forces acting on the Sun. The strength of the Sun's response to planetary forcing depends nonlinearly on the state of internal solar dynamics; planetary-Sun coupling effects are enhanced during solar activity maxima and attenuated during minima.

Keywords: Total solar irradiance modulation; satellite monitoring; time series analysis; planetary solar modulation; non-linear coupling; strong maxima -weak minima.

Submitted 2013.09-27, Accepted 2013-10-30. https://doi.org/10.53234/scc202504/17

-

¹ First published in Pattern < Recognition of Physics, 1, 123-133, doi:10.5194/prp-1-123-2013

1. Introduction

Total solar irradiance (TSI) satellite measurements are fundamental to the investigation of solar physics and the climate change forcing of TSI variability. TSI observations follow the solar magnetic activity level (Willson and Hudson, 1991) and their variation therefore conforms to the ~11 yr Schwabe solar cycle. The average TSI on solar cycle time scales is sometimes referred to as the *solar constant*. TSI records are characterized by complex variability, from the quasi-monthly differential solar rotation cycles to the subannual and annual time scales (whose origins are still unknown).

An important physical issue is whether the annual and subannual TSI variability is intrinsically chaotic and unpredictable or, alternatively, is made of a complex set of harmonics and may be predicted once a sufficient number of constituent harmonics are identified. The latter possibility implies solar activity forecasts and may benefit from harmonic constituent modeling, as have the predictions of ocean tidal levels on Earth using a set of specific solar and lunar orbital harmonics (Doodson, 1921; Kelvin, 1881).

The harmonic constituent model hypothesis is important because it could provide an explanation of many solar magnetic and radiative phenomena that conventional solar physics cannot. The conventional view of solar science is that solar magnetic and radiant variability is intrinsically chaotic, driven by internal solar dynamics alone and characterized by hydromagnetic solar dynamo models (Tobias, 2002). These models cannot predict solar activity and have not been able to explain its complex variability.

A growing body of empirical evidence suggests that solar activity on monthly to millennial time scales may be modulated by gravitational and magnetic planetary harmonic forces (Abreu et al., 2012; Brown, 1900; Charvátová, 2009; FairbridgeandShirley, 1987; Hung, 2007; Jose, 1965; Scafetta, 2010a,b, 2012a,b,c,d; ScafettaandWillson, 2013a; Sharp, 2013; TanandCheng, 2012; Wilson et al., 2008; Wolf, 1859; Wolff and Patrone, 2010, e.g.,). For example, the 11 yr solar cycle appears to be bounded by the Jupiter–Saturn spring tide oscillation period (9.93 yr) and the Jupiter orbital tide oscillation period (11.86 yr) (Scafetta, 2012c). The 11 yr solar cycle is also in phase with major tidal resonances generated by the Venus-Earth-Jupiter system (11.07 yr period) and by the Mercury–Venus system (11.08 yr period) (Scafetta, 2012d). The multidecadal, secular and millennial solar oscillations appear to be generated by beat interferences among the multiple cycles that comprise the 11 yr solar cycles (Scafetta, 2012c).

A recent commentary in *Nature* discusses the "revival" of the planetary hypothesis of solar variation (Charbonneau, 2013). It has been pointed out that the arguments of critics of this hypothesis (Callebaut et al., 2012; Smythe and Eddy, 1977, e.g.,) have either not been supported by empirical evidence or have based their arguments on overly simplistic Newtonian analytical physics (Scafetta, 2012c,d; Scafetta et al., 2013b, e.g.,).

In a previous publication, Scafetta and Willson (2013b) analyzed the power spectra of TSI records since 1992. These were compared with theoretical power spectra deduced from the planetary orbital effects such as the tidal potential on the Sun, and the speed, jerk force, and z axis coordinate of the Sun relative to the barycenter of the solar system. The authors found multiple evidences of spectral coherence on annual and subannual scales between TSI power spectra and theoretical planetary spectra. This suggests that TSI is modulated at specific frequencies by gravitational and/or electromagnetic forcings linked to the revolution of the planets around the Sun.

Scafetta and Willson (2013b) found a TSI signature of the 1.092 yr Earth-Jupiter conjunction cycle. The TSI oscillation was found to be particularly evident during the maximum of solar cycle 23 (1998–2004) and in phase synchronization with the Earth–Jupiter conjunction cycle that predicts an enhanced effect when the Earth crosses the Sun–Jupiter conjunction line. The cause was

postulated to be that a slightly brighter side of the Sun was facing Jupiter, because that side would be the focus of enhanced planetary—solar couplings, both gravitational and electromagnetic. These forces exerted by Jupiter on the Sun are stronger than the force exerted on the Sun by any other planet. When the Earth crosses the Sun–Jupiter conjunction line it adds to Jupiter's planetary—solar coupling effects and sensors on Earth satellites should receive a stronger TSI signal. This planetary—solar coupling effect generates the ~ 1.092 yr cycle in the TSI record.

The 1.092 yr cycle signature detected by the satellite TSI observations is enhanced during solar activity maxima and attenuated during solar minima (Scafetta and Willson, 2013b), suggesting complex, nonlinear responses of solar internal dynamics to planetary forcings. Here we study the dynamical evolution of the harmonic characteristics of the TSI observations on annual and sub annual time scales. A multiscale dynamical spectral analysis technique is proposed and used to reveal non-stationary changes in dynamical patterns in a sequence. This technique is used to determine whether major background harmonics exist that correspond to basic planetary harmonics such as the spring, orbital and synodic periods among the planets.

2. Total Solar Irradiance Data

The daily average TSI measurements were collected during the last decade by three independent science teams: ACRIMSAT/ACRIM3 (Active Cavity Radiometer Irradiance Monitor Satellite/Active Cavity Radiometer Irradiance Monitor 3) (Willson and Mordvinov, 2003), SOHO/VIRGO (Solar and Heliopheric Observatory/Variability of solar Irradiance and Gravity Oscillations) (Fröhlich, 2006), and SORCE/TIM (Solar Radiation and Climate Experiment/Total Irradiance Monitor) (Kopp and Lawrence, 2005; Kopp et al., 2005). Cross-comparison of the three independent TSI records reduces interpretation errors due to measurement uncertainties. Dynamical patterns common to the three TSI records are sought out in order to increase the certainty of their physical origins.

ACRIM3 results have been adjusted using algorithm updates and corrections for scattering and diffraction found in recent testing at the LASP/TRF (Laboratory for Atmospherics and Space Physics/TSI Radiation Facility) (Willson, 2011). Similar corrections for the VIRGO results were recently found at LASP/TRF, and these results are now reported in an updated scale (Fröhlich, 2013). The updated ACRIM3, VIRGO and TIM results agree closely in scale and variability, with an average value during the 2008–2009 solar activity minimum near 1361 W m⁻².

The ACRIMSAT/ACRIM3, SOHO/VIRGO and SORCE/TIM TSI records since 2003 are shown in Fig. 1. For comparison, Fig. 1 also depicts the daily sunspot number record from the Solar Influences Data Analysis Center (SIDC).

Note that Fig. 1 shows the most recent SOHO/VIRGO record available that does not yet include the LASP/TRF scaling corrections. Thus, it is more significant to compare the three TSI records as percentage variation during successive two-year periods as depicted in Figs. 2 and 3.

Figure 2 uses a constant scale for each two-year period to demonstrate the progressive divergence of TIM relative to ACRIM3 and VIRGO results. The three records are scaled during the initial common two-week period (2003.15–2003.19). The close agreement of all three satellite experiments' results in 2003 was followed by continuous divergence of TIM results from those of ACRIM3 and VIRGO through 2013, when the difference reached ~200 ppm.

ACRIMSAT/ACRIM3, SOHO/VIRGO, SORCE/TIM 1368 1360 200 200 2002 2004 2006 2008 2010 2012 2014 year

Figure 1: Comparison of ACRIMSAT/ACRIM3 (black), SOHO/VIRGO (blue) and SORCE/TIM (red) total solar irradiance records versus the SIDC daily sunspot number (gray) record. ACRIM3 is recalibrated with updated sensor degradation and algorithm LAPS/TRF corrections for scattering, diffraction and TSI scale. VIRGO does not include yet the LASP/TRF scaling corrections.

Based on previous satellite TSI observational experience, the most likely cause of the divergence is in-flight sensor degradation calibration error. The close agreement of ACRIM3 and VIRGO results, which is more evident in Figs. 2–3, indicates that an over-correction of TIM sensor degradation is the most likely explanation. However, the cause could also be a combination of degradation uncertainty by all three sensors; or it may be within the uncertainty of the self-degradation calibration capabilities of these instruments. The long-term traceability of TSI satellite results, achieved through in-flight self-calibration of degradation, is an important area of continuing research for the climate TSI database.

Figure 3 uses a variable scale on each two-year segment to provide maximum visibility of the TSI variations for each sensor. It can be clearly seen that ACRIM3, VIRGO and TIM detect nearly all the same variations. TIM appears to detect them as having slightly lower amplitudes. During the part of the solar minimum period with the quietest magnetic activity (2008.7–2009.3) there is a near absence of variations in the TIM record, while VIRGO records some of the variability detected by ACRIM3 during this time, but at lower amplitudes. Lower sensitivities of VIRGO and TIM sensors is likely responsible for these differences.

3. TSI power spectrum comparison

Power spectrum evaluations of the TSI records are shown as Figs. 4, 5 and 6. In the following two subsections we analyze the multi-month scale (0.1–1.1 yr) and the solar differential rotation scale (22–40 days).

Science of Climate Change

Table 1: List of the major theoretically expected harmonics associated with planetary orbits within 1.6 year period. P is the period. Mercury: (Me), Venus: (Ve), Earth: (Ea), Jupiter: (Ju). If P_1 and P_2 are the periods, the synodic period is $P_{12} = 1/|1/P_1|$, and the spring period is half of it. The variability is based on ephemeris calculations. From Scafetta and Willson (2013b).

Cycle	Туре	P (day)	P (year)	min. (year)	max. (year)
Me	1/2 orbital	44 ± 0	0.1205 ± 0.000	0.1205	0.1205
Me-Ju	spring	45 ± 9	0.123 ± 0.024	0.090	0.156
Me-Ea	spring	58 ± 10	0.159 ± 0.027	0.117	0.189
Me-Ve	spring	72 ± 8	0.198 ± 0.021	0.156	0.219
Me	orbital	88 ± 0	0.241 ± 0.000	0.241	0.241
Me-Ju	synodic	90 ± 1	0.246 ± 0.002	0.243	0.250
Ea	1/4 orbital	91 ± 3	0.25 ± 0.000	0.250	0.250
Ve	1/2 orbital	112.5 ± 0	0.3075 ± 0.000	0.3075	0.3075
Me-Ea	synodic	116 ± 9	0.317 ± 0.024	0.290	0.354
Ve-Ju	spring	118 ± 1	0.324 ± 0.003	0.319	0.328
Ea	1/3 orbital	121 ± 7	0.333 ± 0.000	0.333	0.333
Me-Ve	synodic	145 ± 12	0.396 ± 0.033	0.342	0.433
Ea	1/2 orbital	182 ± 0	0.500 ± 0.000	0.5	0.5
Ea-Ju	spring	199 ± 3	0.546 ± 0.010	0.531	0.562
Ve	orbital	225 ± 0	0.615 ± 0.000	0.241	0.241
Ve-Ju	synodic	237 ± 1	0.649 ± 0.004	0.642	0.654
Ve-Ea	spring	292 ± 3	0.799 ± 0.008	0.786	0.810
Ea	orbital	365.25 ± 0	1.000 ± 0.000	1.000	1.000
Ea-Ju	synodic	399 ± 3	1.092 ± 0.009	1.082	1.104
Ea-Ve	synodic	584 ± 6	1.599 ± 0.016	1.572	1.620

ACRIMSAT/ACRIM3, SOHO/VIRGO, SORCE/TIM -0.1 — 2003 2004.75 2003.25 2004 2004.25 2004.5 2003.5 2003.75 2005 0.1 Percent Variation 2005.25 2005.5 2005.75 2006 2006.25 2006.5 2006.75 2007 2007.25 2007.5 2007.75 2008 2008.25 2008.5 2008.75 2009 -0.1 2009.25 2009.5 2009.75 2010.25 2010.5 2010.75 2010 2011 2009 0.1 -0.1 | 2011 2011.5 2011.25 2011.75 2012 2012.25 2012.5 2012.75 2013 year

Figure 2: Percent variation comparison of ACRIMSAT/ACRIM3 (black), SOHO/VIRGO (blue) and SORCE/TIM (red) total solar irradiance records. The scale of the two-year segments is constant to highlight the divergent trend of the TIM results relative to those of the ACRIM3 and VIRGO experiments. The records are cross-scaled during the initial two-week period 2003.15–2003.19.

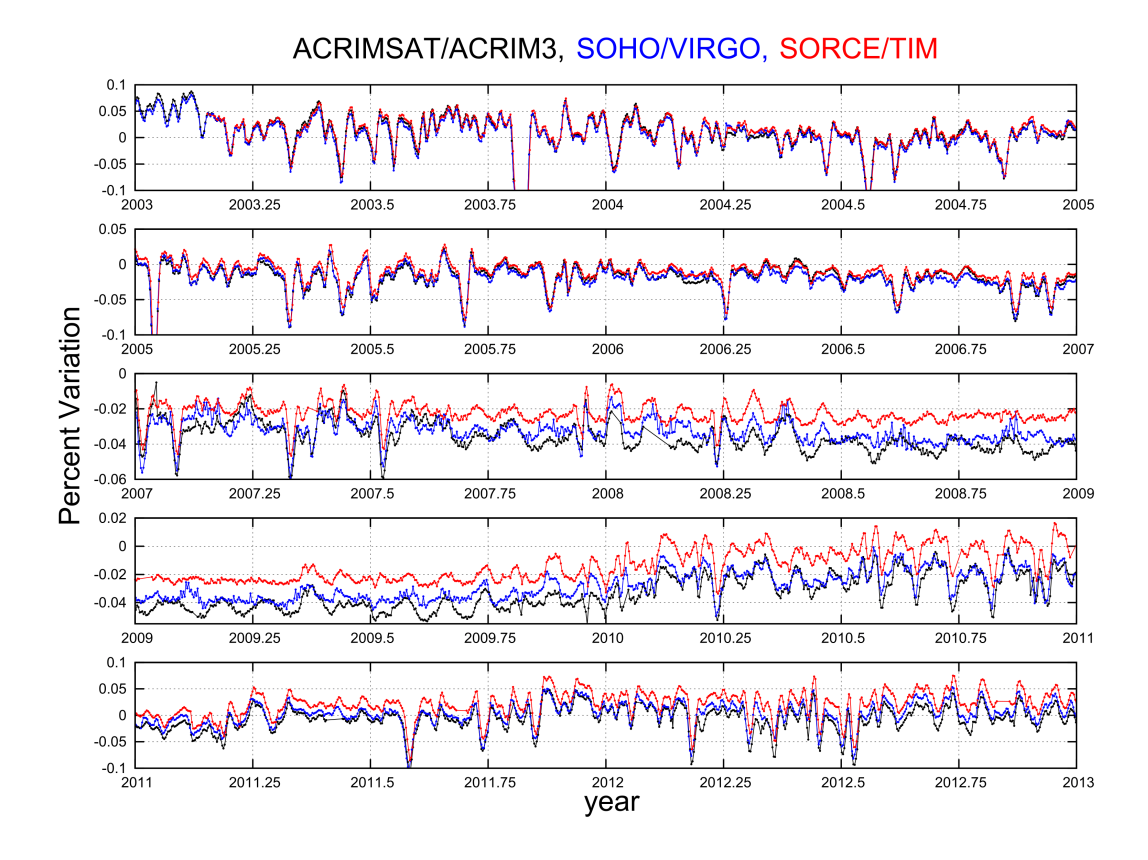


Figure 3: Percent variation comparison of ACRIMSAT/ACRIM3 (black), SOHO/VIRGO (blue) and SORCE/TIM (red) total solar irradiance records. The scale of the two-year segments is varied to highlight the detailed similarity of the variability of all three TSI records. The records are cross-scaled during the initial two-week period 2003.15–2003.19.

3.1 Analysis of the 0.1–1.1 yr period range

Figure 4 shows the maximum entropy method (MEM) power spectrum evaluation (Press et al., 1997) of the ACRIM3, VIRGO and TIM TSI records during the 10 yr period from 2003.15 to 2013.16. The power spectra are plotted as a function of the period (T = 1/f) up to 1 yr. The figure shows that the three records produce nearly all the same spectral peaks, indicating that the observed variations in TSI are definitively solar in origin. The spectral amplitude of the peaks in the ACRIM3 record is nearly always higher than that observed by VIRGO and TIM, indicating a higher sensitivity of ACRIM3 instrumentation to TSI variability. This sensitivity difference is also supported by the fact that the TIM and VIRGO records present slightly smoothed and attenuated patterns relative to those of ACRIM3. The major spectral peaks are highlighted in the figure, and occur at the following approximate periods: ~ 0.070 yr, ~ 0.095 yr, 0.20 yr, 0.25 yr, 0.30-0.34 yr, 0.39 yr and 0.75-0.85 yr; more uncertain peaks occur at about 0.60-0.65 yr.

The above-mentioned periods are found among the major planetary harmonics related to the orbital, synodic and spring periods for the planets. Table 1 reports these periods and their uncertainty and range during 2003–2013 for the four major tide-causing planets (Mercury, Venus, Earth and Jupiter) (Scafetta, 2012d). Table 2 shows theoretically expected periods related to the other planets as well. The major orbital, synodic and spring periods listed in Table 1 are indicated with colored arrows at the top of Fig. 4; red indicates orbital periods, black indicates spring periods,

Science of Climate Change

ACRIMSAT/ACRIM3, SOHO/VIRGO, SORCE/TIM

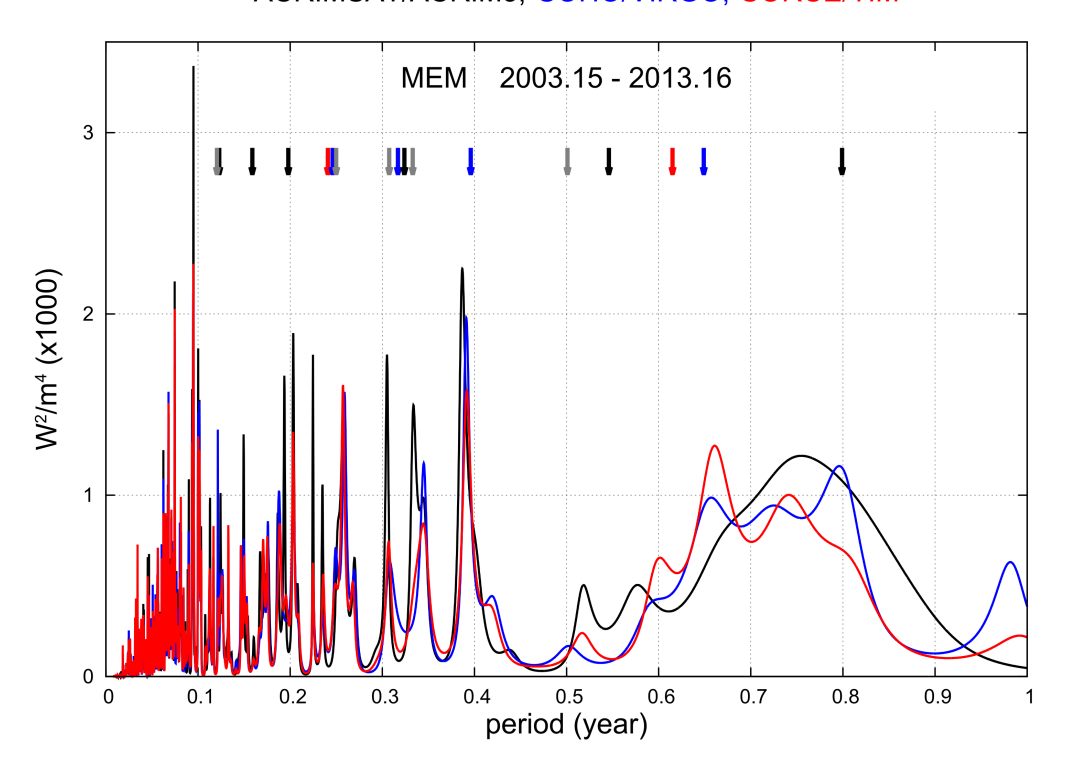


Figure 4: Maximum entropy method (MEM) power spectrum comparison of ACRIMSAT/ACRIM3 (black), SOHO/VIRGO (blue) and SORCE/TIM (red) total solar irradiance records using the data from 2003.15 to 2013.16. The colored arrows at the top of the figure indicate the major theoretically expected planetary frequencies from Mercury, Venus, Earth and Jupiter, which are reported in Table 1. Red indicates the orbital periods, black indicates the spring periods, blue indicates the synodic periods, and gray indicates the harmonics of the orbital periods listed in Table 1.

blue indicates the synodic periods, and gray indicates the harmonics of the orbital periods listed in Table 1. The additional planetary frequencies listed in Table 2 likely have only minor TSI effects and are not explicitly delineated in Fig. 4; we report these additional frequencies for completeness. Although there is currently a deficit of specific physical mechanisms to explain planet—Sun interactions, these minor frequencies may also be found in solar records.

Scafetta and Willson (2013b) found similar frequencies using theoretical equations deduced from the ephemerides of the planets, such as the tidal potential on the Sun and the speed, jerk force, and z axis coordinate of the Sun relative to the barycenter of the solar system. Statistical tests based on Monte Carlo simulations using red-noise generators for TSI synthetic records established that the probability of randomly finding a dynamical sequence manifesting a spectral coherence with the (orbital, spring and synodic)

planetary theoretical harmonics equal to or larger than that found among the TSI satellite frequencies and the planetary harmonics is less than 0.05 % (<u>Scafetta and Willson</u>, <u>2013b</u>).

A comparison between the spectral peaks shown in Fig. 4 and the colored arrows indicating the major expected planetary frequency peaks shows a clear coherence among the TSI and the planetary harmonics on multiple scales, in particular for the periods from 0.1 to 0.5 yr and for the 0.8 yr periodicity. The three planetary periods at about 0.55 yr and between 0.6 and 0.65 yr are not equally evident in the TSI results.

Science of Climate Change

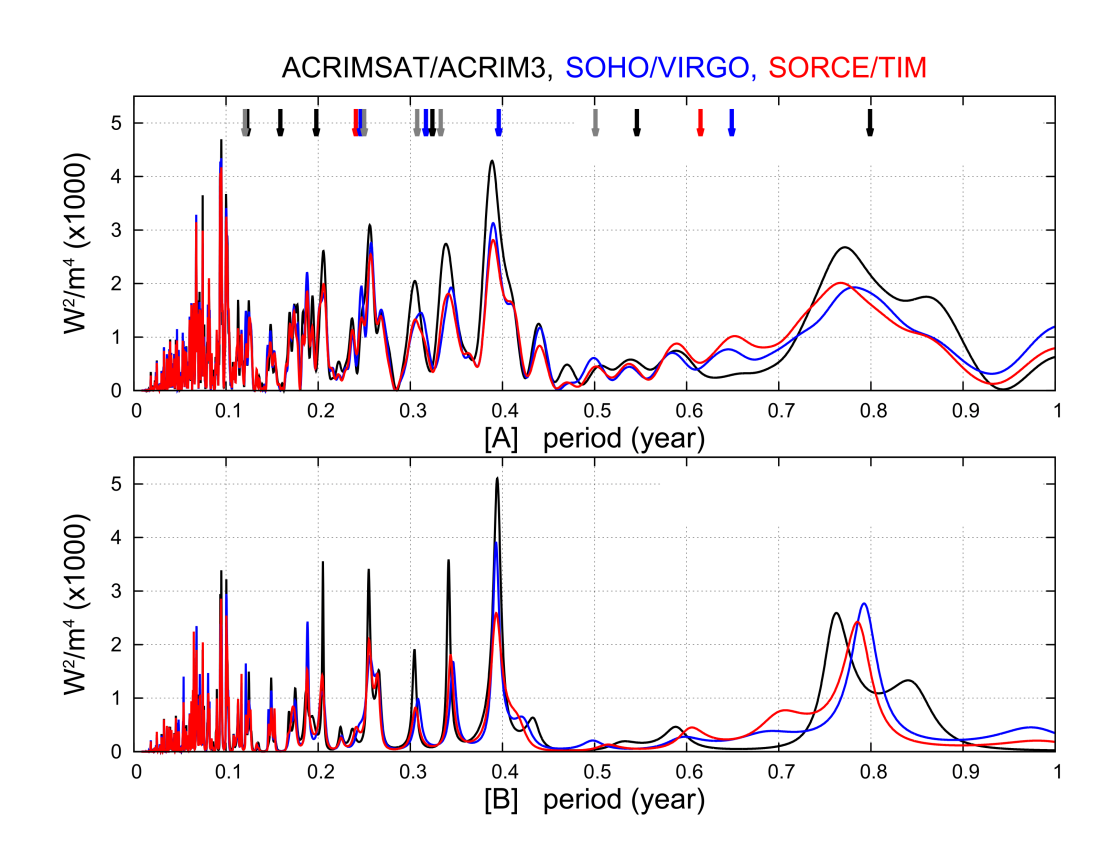


Figure 5: Power spectrum comparison of ACRIMSAT/ACRIM3 (black), SOHO/VIRGO (blue) and SORCE/TIM (red) total solar irradiance records, using the data from 2003.15 to 2011.00. (A) The periodogram is used; (B) the maximum entropy method (MEM) is used. The colored arrows at the top of the figure indicate the major theoretically expected planetary frequencies from Mercury, Venus, Earth and Jupiter, which are reported in Table 1. Red indicates the orbital periods, black indicates the spring periods, blue indicates the synodic periods, and gray indicates the harmonics of the orbital periods listed in Table 1.

As discussed in the Introduction, the response of the Sun to external planetary forcing may be nonlinear with some frequencies enhanced by internal solar dynamics during specific periods (e.g., solar maxima) and attenuated during others (e.g., solar minima). Indeed, changing the analyzed period as done in Fig. 5 (we used the data from 2003.15 to 2011) produces some differences relative to the results depicted in Fig. 4. For example, the amplitudes of the peaks are different, although their frequency position is fairly unchanged. This demonstrates that nonlinear mechanisms are regulating the phenomenon. Section 4 addresses the nonlinear dynamical evolution of the TSI patterns more systematically

3.2 Analysis of the 22–40 day period range associated with the solar differential rotation

Figure 6 magnifies the period between 22 and 40 days depicted in Fig. 4. This range corresponds to the differential solar rotation period band. Figure 6 clearly shows a spectral peak at ~27.3 days (0.075 yr) (Willson and Mordvinov, 1999). This corresponds to the synodic period between the well-known Carrington solar rotation (~25.38 days) and the Earth's orbital period (~365.25 days). The Carrington period roughly corresponds to the solar rotation period at a latitude of 26° from the Sun's equatorial plane, which is the average latitude of sunspots and corresponding magnetic solar activity (Bartels, 1934), as seen from the Earth.

3.5 34.7d 0.095y3 27.3d 2.5 0.075y W^2/m^4 (x1000) ~37d ~0.101y 2 24.8d 0.068y1.5 1 0.5 0 34 period (day) 1

ACRIMSAT/ACRIM3, SOHO/VIRGO, SORCE/TIM

Figure 6: Magnification of the period range between 22 and 40 days depicted in Fig. 4, which is associated with the solar differential rotation scale. The arrows at the bottom depict the solar rotation cycles reported in Table 3.

Figure 6 also reveals spectral peaks at \sim 24.8 days (\sim 0.068 yr), at \sim 34–35 days (\sim 0.093–0.096 yr) and ~36–38 days (~0.099–0.104 yr), suggesting that the sidereal equatorial and polar solar rotation cycles would also be reported in TSI records. However, the presence of these cycles in the TSI records could imply that the solar orientation relative to space also modulates solar activity. An explanation of these spectral peaks could involve a planetary influence on the Sun.

Assuming that the side of the Sun facing Jupiter is the focus of higher solar activity (Scafetta and Willson, 2013b), it is possible to interpret the ~24.8 days (~0.0679 yr) cycle as the synodic period between Jupiter's sidereal orbital period ($\sim 4332.6 \text{ days} = \sim 11.862 \text{ yr}$) and the solar equatorial rotation period. The latter is estimated to be ~ 24.7 days (~ 0.0675 yr) during the period analyzed here (from 2003 to 2013). Using this estimate, additional planetary synodic cycles with the solar rotation are calculated at: ~26.5 days (~0.0725 yr), the synodic solar equatorial rotation period relative to Earth; ~27.75 days (~0.0760 yr), the synodic solar equatorial rotation period relative to Venus; and ~34.3 days (~0.0940 yr), the synodic solar equatorial rotation period relative to Mercury. See Table 3.

The ~34.3-day Mercury–Sun synodic period fits the TSI spectral peak at ~34–35 days, a period that also corresponds to the high latitude solar differential rotation rate. However, the theoretical synodic spectral peaks at ~ 26.5 days and ~ 27.75 days do not appear in Fig. 5. This would suggest that solar asymmetry causes a TSI enhancement as the Sun's more sensitive region orientates only toward Jupiter and Mercury.

Table 2: List of additional average theoretically expected harmonics associated with planetary orbits: Mercury (Me), Venus (Ve), Earth (Ea), Mars (Ma), Jupiter (Ju), Saturn (Sa), Uranus (Ur), Neptune (Ne). If P_1 and P_2 are the periods, the synodic period is $P_{12} = 1/|1/P_1 - 1/P_2|$, and the spring period is half of that (Scafetta and Willson, 2013b). The last five rows report additional spring and synodic periods of Mercury, Venus and Earth relative to the synodic periods of Jupiter and Saturn, and Earth and Jupiter. The latter periods are calculated using the three-synodic-period equation: $P_{1(23)} = 1/|1/P_1 - 1/P_2 - 1/P_3||$.

Cycle	Туре	P (year)	Type	P (year)
Me-Ne	spring	0.1206	synodic	0.2413
Me–Ur	spring	0.1208	synodic	0.2416
Me-Sa	spring	0.1215	synodic	0.2429
Me-Ma	spring	0.1382	synodic	0.2763
Ve-Ne	spring	0.3088	synodic	0.6175
Ve–Ur	spring	0.3099	synodic	0.6197
Ve-Sa	spring	0.3142	synodic	0.6283
Ve-Ma	spring	0.4571	synodic	0.9142
Ea–Ne	spring	0.5031	synodic	1.006
Ea–Ur	spring	0.5060	synodic	1.0121
Ea-Sa	spring	0.5176	synodic	1.0352
Ea–Ma	spring	1.0676	synodic	2.1352
Ma	1/2 orbital	0.9405	orbital	1.8809
Ma-Ne	spring	0.9514	synodic	1.9028
Ma–Ur	spring	0.9621	synodic	1.9241
Ma–Sa	spring	1.0047	synodic	2.0094
Ma–Ju	spring	1.1178	synodic	2.2355
Ju	1/2 orbital	5.9289	orbital	11.858
Ju–Ne	spring	6.3917	synodic	12.783
Ju–Ur	spring	6.9067	synodic	13.813
Ju–Sa	spring	9.9310	synodic	19.862
Sa	1/2 orbital	14.712	orbital	29.424
Sa-Ne	spring	17.935	synodic	35.870
Sa–Ur	spring	22.680	synodic	45.360
Ur	1/2 orbital	41.874	orbital	83.748
Ur–Ne	spring	85.723	synodic	171.45
Ne	1/2 orbital	81.862	orbital	163.72
Me-(Ju-Sa)	spring	0.122	synodic	0.244
Me-(Ea-Ju)	spring	0.155	synodic	0.309
Ve-(Ju-Sa)	spring	0.317	synodic	0.635
Ea-(Ju-Sa)	spring	0.527	synodic	1.053
Ve-(Ea-Ju)	spring	0.704	synodic	1.408

Mercury may have a strong effect because Mercury is the closest planet to the Sun. After Jupiter, Mercury induces on the Sun the second largest tidal amplitude cycle related to a planetary orbit due to its large eccentricity (e = 0.206) and low inclination to the Sun's equator (3.38°) (Scafetta, 2012d, Figure 8). Moreover, the theoretical ~34.3 day Mercury–Sun synodic period has

ACRIMSAT/ACRIM3, SOHO/VIRGO, SORCE/TIM 0.5 W/m^2 -0.5 2004 2006 2008 2010 2012 1 0.5 0 -0.5 -1 2004 2006 2008 2010 2012 0.5 -0.5 2004 2006 2008 2010 2012 year

Figure 7: FFT 2 yr high-pass filtered component of the ACRIMSAT/ACRIM3 (black), SOHO/VIRGO (blue) and SORCE/TIM (red) total solar irradiance records.

an almost 2/5 resonance with Mercury's orbital period (~88 days) or ~35.2 days (~0.096 yr). This close resonance may favor dynamical synchronization and amplification in solar dynamics and explain the wide, strong TSI spectral peak around ~34–35 days that appears bounded by Mercury's two theoretical frequencies, as Fig. 6 shows.

Table 3. Solar equatorial (equ-) and Carrington (Car-) rotation cycles relative to the fixed stars and to the four major tidal planets calculated using the synodic period equation: $P_{12} = 1/|1/P_2 - 1/P_1|$, where $P_1 = 24.7$ days is the sidereal equatorial solar rotation and P_2 the orbital period of a planet. The last row reports the 2/5 Mercury's orbital resonance. The last column reports the color of the arrows shown in Fig. 6.

Cycle	Type	P (day)	P (year)	color
Sun	equ-rot	24.7	0.0676	black
Sun-Ju	equ-rot	24.8	0.0679	red
Sun-Ea	equ-rot	26.5	0.0726	red
Sun-Ea	Car-rot	27.3	0.0747	blue
Sun-Ve	equ-rot	27.8	0.0761	red
Sun-Me	equ-rot	34.3	0.0940	red
2/5 Me	resonance	35.2	0.0964	green

Thus, empirical evidence suggests that the differential solar rotation may be synchronized to the synodic cycles between the solar equatorial rotation and the two theoretically most relevant tidal planets: Jupiter and Mercury. Further investigation of the solar rotation period band requires a dedicated examination that is left to another work.

0.35 0.25 0.2005.5 2006 2006.5 2007 2007.5 2008 2008.5 2009 2009.5 2010 2010.5 201 year

ACRIMSAT/ACRIM3, SOHO/VIRGO, SORCE/TIM

Figure 8: 5 yr moving standard deviation function σ₅(t) of the high-pass filtered ACRIMSAT/ACRIM3 (black), SOHO/VIRGO (blue) and SORCE/TIM (red) total solar irradiance records depicted in Fig. 6

4. Multiscale comparative spectral analysis

Multiscale dynamical spectral analysis diagrams for the three TSI records were constructed as follows. We consecutively calculated normalized power spectrum functions using MEM, which produces sharp peaks and is less affected by leakage artifacts. We processed the TSI records after high-pass filtering to eliminate time scale variations longer than 2 yr. Figure 7 depicts the Fast Fourier Transform (FFT) 2 yr high-pass filtered components of the three TSI records. We analyzed consecutive 5 yr moving centered windows of the data (for example, the results centered in 2006 refer to the 5 yr period from 2003.5 to 2008.5).

Figure 8 shows the 5 yr moving standard deviation functions, $\sigma_5(t)$, of the high-pass filtered TSI records that were used for local normalization of the MEM functions. During the solar minimum, $\sigma_5(t)$ is attenuated relative to the solar cycle 23 and 24 maxima in all three TSI records.

The multiscale comparative spectral analysis diagrams are depicted in Fig. 9 within the period range 0 to 1.1 yr. Figure 10 magnifies the period range from 0.10 to 0.45 yr. The diagrams were obtained by calculating MEM curves for a 5 yr moving centered window and plotting it in a column using colors to represent the strength of the spectral function. For example, the colored column above the year 2006 corresponds to the MEM power spectrum of the data covering the 5 yr period from 2003.5 to 2008.5. The presence of harmonics even when attenuated during solar minimum is emphasized by the colored column in Figs. 9 and 10, which shows a spectrum normalized by the variance $\sigma_5(t)$ of the data during the analyzed 5 yr interval.

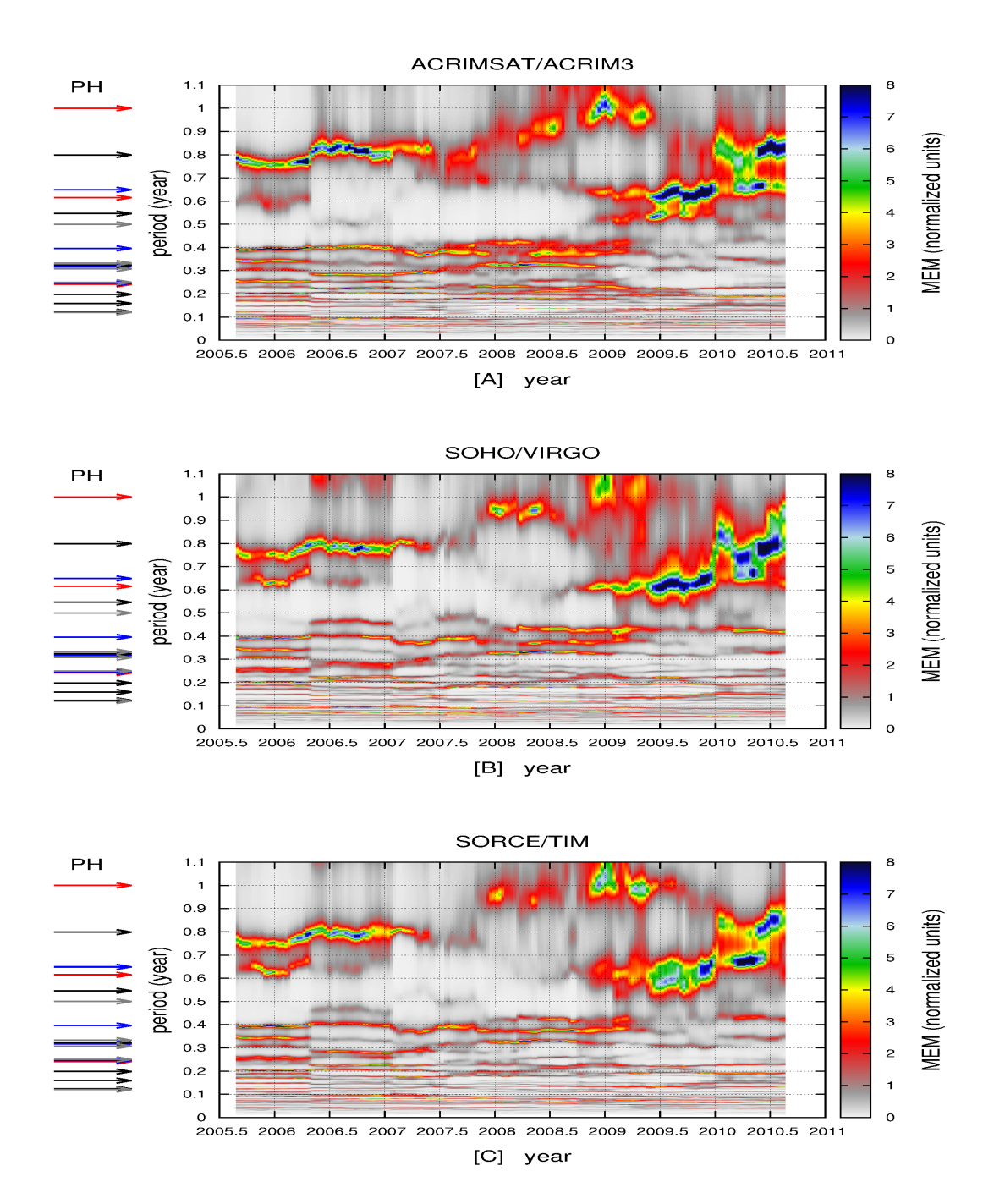


Figure 9: Moving window power spectrum comparison of (A) ACRIMSAT/ACRIM3; (B) SOHO/VIRGO; (C) SORCE/TIM total solar irradiance records. The maximum entropy method (MEM) is used. The colors represent the spectral strength in variance normalized units (×100), with the blue-black regions representing the strongest spectral peaks. The colored arrows at the left of the diagrams indicate the theoretically expected frequencies of the most significant planetary harmonics (PH) obtained from Mercury, Venus, Earth and Jupiter, which are reported in Table 1. Red indicates the orbital periods, black indicates the spring periods, the blue indicates the synodic periods, and gray indicates the harmonics of the orbital periods listed in Table 1

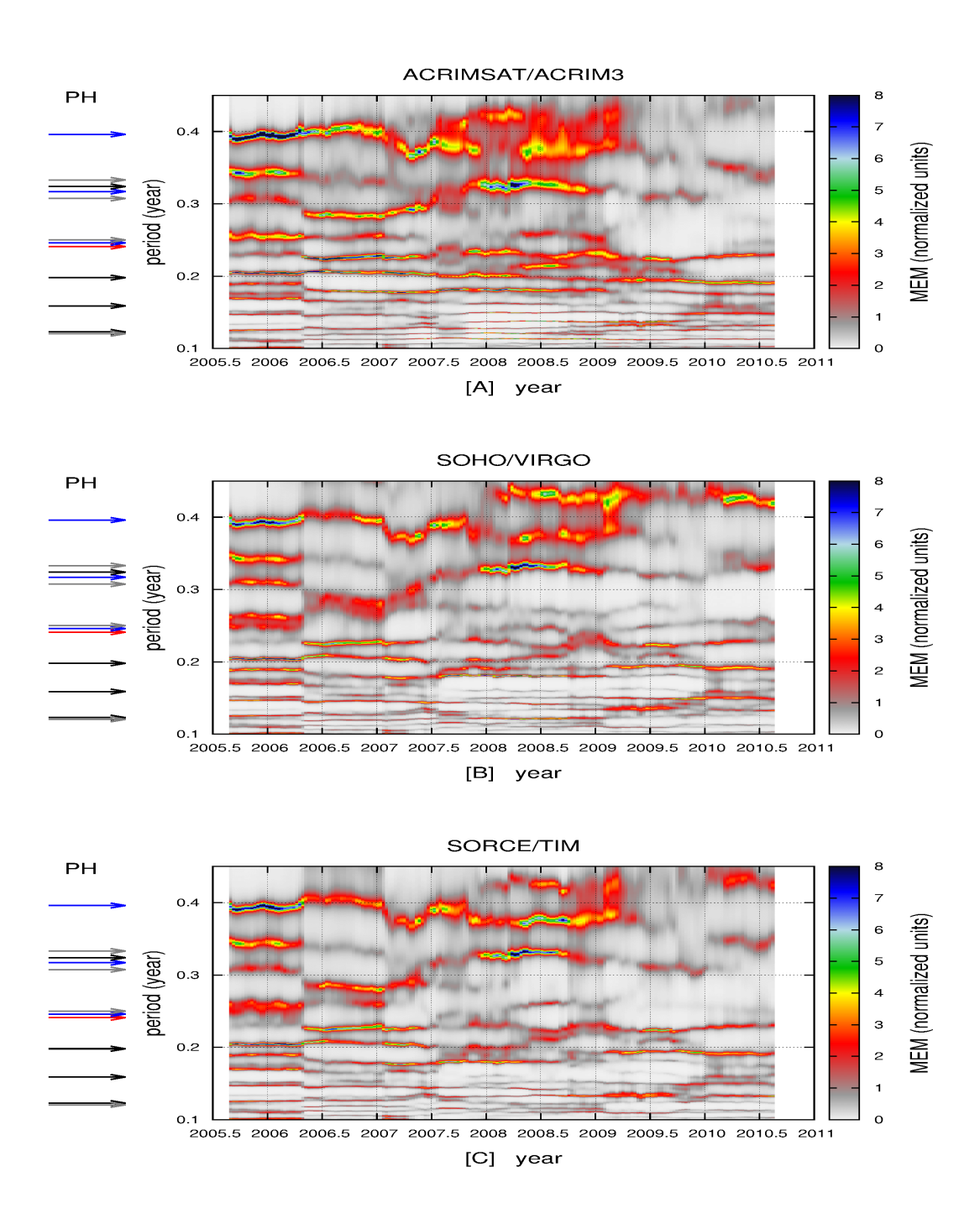


Figure 10: Magnification of Fig. 9 within the frequency period range from 0.10 to 0.45 yr.

Figure 9 shows that even after normalization the amplitude of some frequencies depends strongly on the strength of solar cycle activity. TSI oscillation variability is seen to be larger during solar maxima and smaller during solar minima. Major peaks (blue-black) are observed for the same 5 periodicities seen in Figs. 4 and 5, indicated by arrows on the left. The spectral peaks are relatively stable as the 5 yr window moves in time. The stationarity of these spectral lines increases for periods below 0.5 yr. The peaks near 0.6–0.7 and 0.8 yr are attenuated or disappear during solar cycle 23–24 minimum (~ 2006.75 to 2008.75). The strong periodicities near 0.8 yr are

Science of Climate Change

https://scienceofclimatechange.org

attenuated or disappear during 2008–2009.25. In particular the peak at 0.6–0.65 yr is clearly visible before 2006.5 and after 2008.75 in all three diagrams.

Some differences can also be seen in the three panels of Figs. 9 and 10. The ACRIM3 panel is the most colorful, indicating the highest detection of variability, and TIM is the least colorful (corresponding to the standard deviation variability depicted in Fig. 8). Because the calculations are the same for all three TSI records, this implies that the spectral peaks detected by ACRIM3 are generally stronger that those detected by the other two instruments, providing another confirmation that ACRIM3 sensors are more sensitive than those of VIRGO and TIM, recording stronger signals on multiple scales.

5. Discussion and conclusions

ACRIMSAT/ACRIM3, SOHO/VIRGO and SORCE/TIM TSI records overlap since 2003.15 and are found to be closely correlated with each other. Including the LASP/TRF calibration corrections for both ACRIM3 and VIRGO, all three records present a similar TSI average at about 1361 W m⁻². Figure 1 still depicts the SOHO/VIRGO record on an uncorrected scale (at about 1365 W m⁻²) since the updated VIRGO record is not currently available.

Power spectrum and multiscale dynamical spectral analysis techniques have been used to study the physical properties of these data. We found that TSI is modulated by major harmonics at: $\sim 0.070 \text{ yr}$, $\sim 0.097 \text{ yr}$, $\sim 0.20 \text{ yr}$, $\sim 0.25 \text{ yr}$, $\sim 0.30-0.34 \text{ yr}$, $\sim 0.39 \text{ yr}$; the peaks occurring at $\sim 0.55 \text{ yr}$, $\sim 0.60-0.65 \text{ yr}$ and $\sim 0.7-0.9 \text{ yr}$ appear to be amplified during solar activity cycle maxima and attenuated during the minima.

Other researchers have studied the fast oscillations of alternative solar indices and found results compatible with ours. Rieger et al. (1984) found that an index of energetic solar flare events presents a major variable oscillation with a period of about 154 days (0.42 yr). Similarly, Verma et al. (1992) found a 152–158 day (0.41–0.43 yr) periodicity in records of solar nuclear gamma ray flares and sunspots. This period approximately corresponds to the Mercury-Venus synodic cycle(~0.4 yr), which is quite evident in Figs. 4 and 5, and may slightly vary in time as shown in Figs. 9 and 10. Pap et al. (1990) analyzed a number of solar indices (ACRIM1 TSI, 10.7 cm radio flux, Ca-K plage index, sunspot-blocking function, and UV flux at $L\alpha$, and MgII core-to-wing ratio) and found major spectral peaks at about 51 days (~0.14 yr), 113-117 days (0.30-0.32 yr), 150–157 days (0.41–0.43 yr), 227 days (~0.62 yr) and 240–330 days (0.65–0.90 yr). Caballero and Valdés-Galicia (2003) analyzed the fluctuations detected in high-altitude neutron monitor, solar and interplanetary parameters. Kilcik et al. (2010) analyzed periodicities in solar flare index for solar cycles 21–23. Tan and Cheng (2012) analyzed the solar microwave emission flux at a frequency of 2.80 GHz (F10.7) and the daily relative sunspot number (RSN) from 1 January 1965 to 31 December 2011. These three studies revealed major periodicities within the following period ranges: 53–54 days (0.14–0.15 yr); 85–90 days (0.23–0.25 yr); 115–120 days (0.31–0.33 yr); 140–150 days (0.38–0.41 yr); 230–240 days (0.62–0.66 yr); 360–370 days (0.98–1.02 yr); 395– 400 days (1.08–1.10 yr). The periodicity ranges found above correspond well to those found in the TSI satellite records as shown in Figs. 4, 5, 9 and 10, and correspond to major (orbital, spring and synodic) planetary harmonics as reported in Tables 1 and 2.

Four main high-frequency periods at \sim 24.8 days (\sim 0.068 yr), \sim 27.3 days (\sim 0.075 yr), at \sim 34–35 days (\sim 0.093–0.096 yr) and \sim 36–38 days (\sim 0.099–0.104 yr) characterize the differential solar rotation. The \sim 27.3 days (\sim 0.075 yr) period is the well known Earth's synodic period with the Carrington solar rotation period (\sim 25.38 days). The interpretation of the other cycles is uncertain. Perhaps the \sim 24.8 days (\sim 0.068 yr) and \sim 34–35 days (\sim 0.093–0.096 yr) cycles are the synodic cycles between the equatorial solar rotation cycle and the orbit of Jupiter and Mercury, respectively. The latter could also be synchronized to the 2/5 resonance of the Mercury orbital period of

 \sim 35.2 days (\sim 0.096 yr). The \sim 36–38 days (\sim 0.099–0.104 yr) may be the upper bound of the polar differential solar rotation as seen from the Earth.

In conclusion, solar activity appears to be characterized by the specific major theoretical harmonics, which would be expected if the planets are modulating it. Mercury, Venus, Earth and Jupiter would provide the most modulation within the studied time scales (Scafetta, 2012c,d; Tan and Cheng, 2012). If these planets are modulating solar activity via gravitational and/or electromagnetic forces – although the physical mechanisms are still unknown – the harmonics referring to the spring, orbital and synodic periods among the planets should be present in the TSI records as well. The planetary harmonics reported in Tables 1 and 3, computed using the orbital periods of four theoretically most relevant planets (Mercury, Venus, Earth and Jupiter) correspond very closely to the harmonics observed in the TSI records (see Figs. 4, 5, 6, 9 and 10).

Our findings support the hypothesis that planetary forces are modulating solar activity and TSI on multiple time scales. Scafetta proposed a physical mechanism that may explain how the small energy dissipated by the gravitational tides may be significantly amplified up to a 4-million factor by activating a modulation of the solar nuclear fusion rate (Scafetta, 2012d). However, the additional presence of theoretical synodic cycles and an 11 yr solar cycle modulation of the subannual TSI variability also suggest electromagnetic planet—Sun interactions that could more directly drive the solar outer regions. Thus, if the planets are modulating solar activity as our analysis suggests, the solar response to planetary forcing would be complex and would nonlinearly depend on the 11 yr solar cycle. Further research is required to investigate the physical mechanisms of planetary—solar interactions and construct models capable of simulating and predicting solar activity and TSI variability.

A Appendix

The data were downloaded from the following websites:

- ACRIMSAT/ACRIM3: http://acrim.com/RESULTS/data/acrim3/daya2sddeg_ts4_Nov_2013_hdr.txt
- SOHO/VIRGO: <u>ftp://ftp.pmodwrc.ch/pub/data/irradiance/virgo/TSI/virgo_tsi_d_v6_002_1302.dat</u>
- SORCE/TIM: http://lasp.colorado.edu/data/sorce/tsi_data/daily/sorce_tsi_L3_c24h_latest.txt
- SSN: http://sidc.oma.be/silso/DATA/dayssn import.dat

Editor: N-A. Mörner; Reviewers: two anonymous.

Acknowledgements

The National Aeronautics and Space Administration supported R. C. Willson under contract NNG004HZ42C at Columbia University, and subcontracts 1345042 and 1405003 at the Jet Propulsion

References

- Abreu, J. A. 2012, Beer, J., Ferriz-Mas, A., McCracken, K. G., and Steinhilber, F.: *Is there a planetary influence on solar activity?* Astron. Astrophys., 548, A88, DOI:10.1051/0004-6361/201219997.
- Bartels, J. '934: Twenty-seven day recurrences in terrestrial-magnetic and solar activity, 1923–1933, J. Geophys. Res., 39, 201–202a, DOI:10.1029/TE039i003p00201
- Brown, E. W. 1900: *A Possible Explanation of the Sun-spot Period*, Mon. Not. R. Astron. Soc., 60, 599–606.
- Caballero, R. and Valdés-Galicia, J. F. 2003: Statistical Analysis of the Fluctuations Detected in High-Altitude Neutron Monitor, Solar and Interplanetary Parameters, Sol. Phys., 213, 413–426.
- Callebaut, D. K., de Jager, C., and Duhau, S. 2012: *The influence of planetary attractions on the solar tachocline*, J. Atmos. Sol.-Terr. Phy., 80, 73–78.
- Charbonneau, P. 2013: Solar physics: The planetary hypothesis revived, Nature, 493, 613–614.
- Charvátová, I. 2009: Long-term predictive assessments of solar and geomagnetic activities made on the basis of the close similarity between the solar inertial motions in the intervals 1840–1905 and 1980–2045, New Astron., 14, 25–30.
- Doodson, A. T. 1921: *The harmonic development of the tide-generating potential*, P. Roy. Soc. Lond. A, 100, 305–329.
- Fairbridge, R. W. and Shirley, J. H. 1987: Prolonged minima and the 179-year cycle of the solar inertial motion, Sol. Phys., 10, 191–210.
- Fröhlich, C. 2006: Solar irradiance variability since 1978: revision of the PMOD composite during solar cycle 21, Space Sci. Rev., 125, 53–65.
- Fröhlich, C. 2013: *Revised characterization of the PMO6V radiometers*, ISSI, Bern, Switzerland, 14 May.
- Hung, C.-C. 2007: Apparent Relations Between Solar Activity and Solar Tides Caused by the Planets, NASA/TM-2007-214817.
- Jose, P. D. 1965: Sun's motion and sunspots, Astron. J., 70, 193-200.
- Kelvin (Lord, Thomson, W.) 1881: *The tide gauge, tidal harmonic analyzer, and tide predictor*, P. I. Civil Eng., 65, 3–24.
- Kilcik, A., Özgüc, A., Rozelot, J. P., and Atas, T. 2010: Periodicities in solar flare index for cycles 21–23 revisited, Solar Phys., 264, 255–268,.
- Kopp, G. and Lawrence, G. 2005: *The Total Irradiance Monitor (TIM): Instrument, Design*, Sol. Phys., 230, 91–109.
- Kopp, G., Heuerman, K., and Lawrence, G.2005: *The Total Irradiance Monitor; (TIM): Instrument Calibration*, Sol. Phys., 230, 111–127.
- Pap, J., Tobiska, W. K., and Bouwer, S. D. 1990: *Periodicities of solar irradiance and solar activity indices, I.*, Sol. Phys., 129, 165–1890.
- Press, W. H., Teukolsky, S. A., Vetterling, W. T., and Flannery, B. P. 1997: *Numerical Recipes in C*, 2nd Edn., Cambridge University Press.
- Rieger, E., Kanbach, G., Reppin, C., Share, G. H., Forrest, D. J., and Chupp, E. L. 1984: *A 154-day periodicity in the occurrence of hard solar flares?*, Nature, 312, 623–625.

- Scafetta, N. 2010a: *Empirical evidence for a celestial origin of the climate oscillations and its implications*, J. Atmos. Sol.-Terr. Phy., 72, 951–970, DOI:10.1016/j.jastp.2010.04.015.
- Scafetta, N. 2010b: Spectral analysis of the TSI satellite records, their comparison and interpretation. Abstract #{}GC21B-0868(presented at 2010 Fall Meeting, AGU, San Francisco, Calif., 13–17 December 2010).
- Scafetta, N. 2012a: A shared frequency set between the historical mid-latitude aurora records and the global surface temperature, J. Atmos. Sol.-Terr. Phy., 74, 145–163, DOI:10.1016/j.jastp.2011.10.013.
- Scafetta, N.2012b: Testing an astronomically based decadal-scale empirical harmonic climate model versus the IPCC (2007) general circulation climate models, J. Atmos. Sol.-Terr. Phy., 80, 124–137, DOI:10.1016/j.jastp.2011.12.005.
- Scafetta, N. 2012c: Multi-scale harmonic model for solar and climate cyclical variation throughout the Holocene based on Jupiter-Saturn tidal frequencies plus the 11-year solar dynamo cycle, J. Atmos. Sol.-Terr. Phy., 80, 296–311, DOI:10.1016/j.jastp.2012.02.016.
- Scafetta, N. 2012d: Does the Sun work as a nuclear fusion amplifier of planetary tidal forcing? A proposal for a physical mechanism based on the mass-luminosity relation, J. Atmos. Sol.-Terr. Phy., 81–82, 27–40, DOI:10.1016/j.jastp.2012.04.002.
- Scafetta, N. and Willson, R. C. 2013a: *Planetary harmonics in the historical Hungarian aurora record (1523–1960)*, Planet. Space2013b Sci., 78, 38–44, DOI:10.1016/j.pss.2013.01.005.
- Scafetta, N. and Willson, R. C. 2013b: *Empirical evidences for a planetary modulation of total solar irradiance and the TSI signature of the 1.09-year Earth-Jupiter conjunction cycle*, Astrophys. Space Sci., DOI:10.1007/s10509-013-1558-3, in press, 2013b.
- Scafetta, N., Humlum, O., Solheim, J.-E., and Stordahl, K.: 2013, Comment on "The influence of planetary attractions on the solar tachocline" by Callebaut, de Jager and Duhau, J. Atmos. Sol.-Terr. Phy., 102, 368–371, DOI:10.1016/j.jastp.2013.03.007.
- Sharp, G. J. 2013: Are Uranus & Neptune Responsible for Solar Grand Minima and Solar Cycle Modulation? Int. J. Astron. Astrophys., 3, 260–273.
- Smythe, C. M. and Eddy, J. A. 1977: Planetary tides during Maunder sunspot minimum, Nature, 266, 434–435, 1977.
- Tan, B. and Cheng, Z.: *The mid-term and long-term solar quasi-periodic cycles and the possible relationship with planetary motions*, Astrophys. Space Sci., 343, 511–521, 2013.
- Tobias, S. M.: The Solar Dynamo, Phil. Trans. A, 360, 2741–2756, 2002.
- Verma, V. K., Joshi, G. C., and Paliwal, D. C. 1992: Study of periodicities of solar nuclear gamma ray flares and sunspots, Sol. Phys., 138, 205–208.
- Willson, R. C. 2011: Revision of ACRIMSAT/ACRIM3 TSI results based on LASP/TRF diagnostic test results for the effects of scattering, diffraction and basic SI scale traceability, (Poster GC21C-04), 2011 AGU Fall Meeting.
- Willson, R. C. and Hudson, H. S. 1991: *The Sun's Luminosity Over a Complete Solar Cycle, Nature, 351, 42–44.*
- Willson, R. C. and Mordvinov, V. 1999: *Time-Frequency Analysis of Total Solar Irradiance Variations*, Geophys. Res. Lett., 26, 3613–3616, DOI:10.1029/1999GL010700.
- Willson, R. C. and Mordvinov, V. 2003: Secular total solar irradiance trend during solar cycles 21–23, Geophys. Res. Lett., 30, 1199, DOI:10.1029/2002GL016038.

- Wilson, I. R. G., Carter, B. D., and Waite, I. A. 2008: *Does a Spin-Orbit Coupling Between the Sun and the Jovian Planets Govern the Solar Cycle*?, Publ. Astron. Soc. Aust., 25, 85–93.
- Wolf, R. 1859: Extract of a letter to Mr. Carrington, Mon. Not. R. Astron. Soc., 19, 85–86.
- Wolff, C. L. and Patrone, P. N. 2010: A new way that planets can affect the Sun, Sol. Phys., 266, 227–246.